



HAL
open science

Effect of surfactant concentration and monomer polarity on particle nucleation in emulsion step polymerization of dithiol with diene

Cuong Minh, Marc Schmutz, Abraham Chemtob

► To cite this version:

Cuong Minh, Marc Schmutz, Abraham Chemtob. Effect of surfactant concentration and monomer polarity on particle nucleation in emulsion step polymerization of dithiol with diene. *Colloid and Polymer Science*, 2022, 10.1007/s00396-022-04993-z . hal-03694786

HAL Id: hal-03694786

<https://hal.science/hal-03694786v1>

Submitted on 14 Jun 2022

HAL is a multi-disciplinary open access archive for the deposit and dissemination of scientific research documents, whether they are published or not. The documents may come from teaching and research institutions in France or abroad, or from public or private research centers.

L'archive ouverte pluridisciplinaire **HAL**, est destinée au dépôt et à la diffusion de documents scientifiques de niveau recherche, publiés ou non, émanant des établissements d'enseignement et de recherche français ou étrangers, des laboratoires publics ou privés.

Effect of Surfactant Concentration and Monomer Polarity on Particle Nucleation in Emulsion Step Polymerization of Dithiol with Diene

Cuong Minh Quoc Le,^{1,2} Marc Schmutz³ and Abraham Chemtob^{1,2}*

¹ Université de Haute-Alsace, CNRS, IS2M UMR7361, F-68100 Mulhouse, France

² Université de Strasbourg, France

³ Institut Charles Sadron, CNRS, UPR 22, Université de Strasbourg, 23 Rue du Loess, BP 84047, 67034 Strasbourg, Cedex 2, France

* To whom correspondence should be addressed: abraham.chemtob@uha.fr, +33 3 8960 8834.

Abstract

The dependence of the number of particles N_p as a function of the surfactant concentration $[S]$ is investigated for the step polymerization of dithiol-diene emulsions. A sigmoidal curve for $\log N_p$ vs $\log [S]$ is found for a range of monomers regardless of their polarity. Above the critical micellar concentration (6-20 mM), a $N_p \propto [S]^x$ relationship is established with an exponent x dependent on the polarity of the two co-monomers. When the two co-monomers are highly water insoluble, x varies typically between 0.6 and 1. With two relatively water soluble co-monomers, x is close to 0. When two co-monomers with contrasting water solubility are involved, the power dependence is more difficult to predict and ranges from 0 to 1, but high x value are generally found when one of the two monomers is highly hydrophobic. This overall trend can be reconciled with the behavior of a conventional emulsion radical chain polymerization.

Keywords: emulsion polymerization, thiol-ene, number of particles, particle size

Introduction

In emulsion polymerization, a detailed understanding of the mechanisms governing particle formation is essential because they dictate one of the most important properties of a latex, the number (density) of polymer particles formed (N_p) [1]. This intensive quantity is a major determinant of the particle size, the rate and degree of polymerization. N_p control is also important for reproducibility of latex preparation. Insights given by mechanistic approaches and experimental methods have been instrumental in understanding the way the particles are created for a radical chain polymerization [2]. In a batch polymerization which is the most documented process, particle nucleation is considered to proceed by two main mechanisms [3]. *Micellar nucleation* takes place when oligomeric radicals from the aqueous phase enter monomer-swollen surfactant micelles where propagation will continue. By contrast, in a *homogeneous(-coagulative) nucleation*, the same radicals react with monomer molecules dissolved in the aqueous phase, and precipitate subsequently above a critical size to form precursor particles evolving into mature particles after a number of coalescence events. The relative extent of each mechanism is difficult to establish and depends mainly on the surfactant concentration and the monomer water solubility [4].

Regardless of which particle formation mechanism is dominant, the more important issue, at least from the practical viewpoint, is to be able to predict the quantitative dependence of N_p on the surfactant concentration [S], the initiator concentration [I] and the monomer used. There has been an extensive literature on this subject for radical chain polymerization [5-14] since the pioneering work of Smith and Ewart [15]. Originally, these latter showed that for a dominant micellar nucleation, N_p was proportional to [I] and [S] to the power 0.4 and 0.6, respectively. Although [I] has significant influence on N_p , [S] remains the strongest and the most investigated factor since this latter also affects the colloidal stability of the latex. Subsequent works criticized the dependence on the 0.6 power of the surfactant concentration, and demonstrated that the relationship $N_p \propto [S]^{0.6}$ could be also obtained when *homogeneous nucleation* occurs, and thus cannot be used as evidence of a prevalent micellar nucleation [5, 16]. Fitch, Gardon, Sutterlin, El-Aasser and other authors reported experimental data above Critical Micellar Concentration (CMC) showing $N_p \propto [S]^x$ with an exponent x varying between 0 and 1 depending on the monomer water solubility and the surfactant type. In general, *the dependence of $x = 0.6$ is found for monomers of low water solubility, and up to a limiting [S], whereas x decreases down to zero for monomers with increasing water solubility* [17-19]. With a few exceptions, this trend is generally observed in a radical chain polymerization and provides important guidance for formulators since most emulsion processes are performed in the range $CMC < [S] < 4 \times CMC$. For a typical anionic surfactant such as sodium dodecyl sulfate (SDS), the concentration used in emulsion polymerization is usually in the range 6-24 mM [20-23].

With the recent progress of step polymerizations in emulsion [24], such as thiol-ene emulsion polymerization [25, 26], it is important to revisit the dependence of N_p on [S] [27]. Unlike a chain polymerization, the polymer molecular weight in a step linear polymerization increases very slowly with reaction time (extent of reaction). This means that longer reaction times may be needed to obtain a population of oligomeric radicals able to enter a micelle (*micellar nucleation*) or precipitate in the aqueous phase (*homogeneous nucleation*). While the expected consequence is a delayed nucleation, it is more difficult to predict how the final number of particles will change with

the surfactant concentration. In a first study, we reported that for the batch emulsion polymerization of diallyl phthalate (**DAP**) with 2,2-(ethylenedioxy)diethanedithiol (**EDDT**) using SDS as surfactant, there was almost no change of N_p with $[S]$ above the CMC ($x \sim 0$) (**Figure 1**) [26]. This result is in line with the overall behavior described previously since **EDDT** shows a high water solubility ($s(\text{EDDT}) = 72 \text{ mM}$). In order to gain a more complete picture of the particle formation in emulsion step polymerization, this approach must be extended in terms of surfactant concentration and monomer. The objective is to establish whether or not there is a predictable dependence of N_p with $[S]$. If so, the question is whether the behavior deviates markedly from that described in chain radical polymerization. In this study, the dependence of N_p on $[S]$ in the emulsion step polymerization of dithiol with diene has been thoroughly investigated over a wide range of SDS concentrations below and above the CMC, and using a set of thiol and ene monomers of variable water solubility.

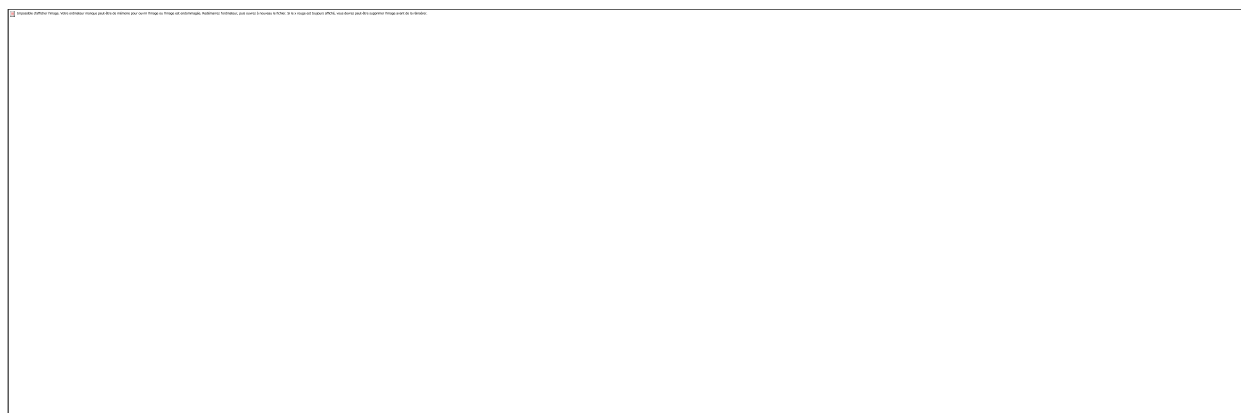


Figure 1. Principle of thiol-ene step polymerization of aqueous emulsion containing a stoichiometric amount of dithiol and diene monomers. Emulsion polymerization of **DAP** with **EDDT** shows little dependence of N_p on surfactant concentration in the region above the CMC.

Experimental section

1. Materials

All monomers were used as received including diallyl phthalate (**DAP**, TCI, 99%), diallyl terephthalate (**DATP**, TCI, 99.4%), diallyl isophthalate (**DAIP**, TCI, 99.7%), diallyl adipate (**DAA**, TCI, 99.8%), di(ethylene glycol) divinyl ether (**DVE**, BASF), 1,4-bis[(vinylloxy)methyl]cyclohexane (**CHDM**, BASF, > 98%), 2,2-(ethylenedioxy)diethanedithiol (**EDDT**, TCI, 99.6%), DL-dithiothreitol (**DTT**, TCI, > 98%), ethylene glycol bismercaptoacetate (**GDMA**, TCI, 97.5%), ethylene glycol bis(3-mercaptopropionate) (**GDMP**, TCI, 98.1%), 2,2'-thioldiethanethiol (**DMDS**, Bruno Bock, 98.7%), 1,6-hexanedithiol (**HMDT**, TCI, 99.1%). 2,5-Di-tert-butylhydroquinone (**DBHQ**, TCI, 99.3%) was used a radical stabilizer for the thiol-ene monomer mixture. The aqueous phase was comprised of sodium dodecyl sulfate (**SDS**, TCI, 98%) as surfactant, lithium phenyl(2,4,6-trimethylbenzoyl)phosphinate (**TPO-Li**, TCI, 99.3%) as water soluble radical photoinitiator and double distilled

water. Dimethyl sulfoxide-d₆ (DMSO-d₆, 99.5% D) was purchased from Eurisotop and other analytical grade solvents were used without further purification.

2. Synthesis

A stoichiometric amount of dithiol and diene was mixed in a 20 mL glass vial in the presence of a radical stabilizer ([DBHQ] = 50 mM respect to monomer volume). Separately, an aqueous phase was prepared containing various concentrations of surfactant ([SDS] from 0.1 to 200 mM) and a fixed concentration of photoinitiator ([TPO-Li] = 7.5 mM). To a 20 mL soda-lime glass vial (outer diameter: 25 mm, height: 70 mm) were added 1.00 g of thiol-ene monomer mixture and 9 g of aqueous phase. The biphasic medium was homogenized with an Ultra-Turrax® T25 homogenizer (IKA-Werke) at 15 000 rpm for 5 min to form a macroemulsion (the probe was immersed to about 1 cm above the bottom of the vial to avoid foaming). The as-prepared macroemulsion being relatively unstable, it was photopolymerized immediately after preparation. Photopolymerization was performed by placing the 20 mL soda-lime glass vial containing the thiol-ene monomer emulsion at the center of a LED circular photochemical reactor constructed by winding a 385 nm LED strip (SMD3528, 60 LED/meter, LightingWill, 3.7 mW·cm⁻²) around a quartz cylinder (inner diameter: 80 mm, length: 100 mm). The experimental set-up is shown in **Fig. S1** of supporting information (SI). Irradiation was carried out at room temperature for 20 min under magnetic stirring (1100 rpm). After the reaction, ene conversion, molecular weight, and particle size of the latex were characterized by different techniques.

3. Characterization

¹H NMR spectroscopy. The final ene-conversion of the emulsion photopolymerization was determined by ¹H-NMR using a 300-MR (Varian) [26]. Practically, a 30 µL aliquot of the latex was dissolved in 0.57 mL of DMSO-d₆.

Dynamic light scattering (DLS) measurement. Particle size and its distribution were determined using a VASCO particle size analyzer (Cordouan, France) featuring a laser source at 658 nm and a detector set to a scattering angle of 135°. Before analysis, the latexes were diluted 100 times in deionized water to reach 0.1 wt% prior measurement. The diluted sample was transferred to DLS cell, and the Dual Thickness Controller (DTC) was set at DOWN. Each sample was acquired 10 times in statistical mode with the signal-to-noise limit of 1 %. The (harmonic) z-average diameter $D_z(TEM)$ was computed by NanoQ software version 2.6 using cumulative data analysis mode. The number-average particle size distributions were also calculated by the software and these raw data were exported to a spreadsheet to calculate the volume-average particle diameter: $D_v(DLS) = \sqrt[3]{\frac{\sum(n_i \times D_i^3)}{n_i}}$ where n_i is the number of particles of diameter D_i . The number of particle per L water of the latex (N_p) was then derived from $D_v(DLS)$ as follow: $N_p = \frac{6 \times m_{mon} \times x}{\pi \times D_v(DLS)^3 \times \rho_{pol} \times V_{aq}}$ where m_{mon} is the mass of thiol and ene monomers (g), x is the conversion in ene group, V_{aq} is the aqueous phase volume (L,) and ρ_{pol} is the volumetric mass density of the polymer (g cm⁻³) [28] [29]. As regards the plot N_p as a function of [S], each point corresponding to specific SDS

concentration was obtained with a minimum of ten DLS measurements to calculate $D_v(DLS)$, then an average of N_p reported as $\overline{N_p} \pm SD$ with SD the standard deviation.

Cryogenic transmission electron microscopy (cryo-TEM). A drop of 5 μL diluted latex sample (0.1 – 1 wt%) was applied to a copper grid covered with a carbon film made hydrophilic using an ELMO glow discharge device (Cordouan Technologies, France). The grid was placed in a home-made freezer at 22°C and 80% relative humidity before plunging into liquid ethane maintained at -190°C by liquid nitrogen. The grid was mounted on a cryo holder (Gatan 626, USA) and observed under low dose conditions in a Tecnai G2 microscope (FEI, The Netherlands) at 200 kV. Images were acquired using an Eagle slow scan CCD camera (FEI). Particle size analysis of the cryo-TEM images was performed using ImageJ software. Images were processed with bandpass Filter function to improve contrast, and particle diameters were automatically detected by using the DetectCircles1.2 plugin. Undetected particles were counted manually. A representative example of automatic particle detection was provided in **Fig. S2** of SI. The number-average diameter ($D_n(TEM) = \sum n_i D_i / \sum n_i$, where n_i is the number of particles of diameter D_i), the weight-average diameter ($D_w(TEM) = \sum n_i D_i^4 / \sum n_i D_i^3$), the z-average diameter ($D_z(TEM) = \sum n_i D_i^6 / \sum n_i D_i^5$), the volume-average diameter $D_v(TEM) = \sqrt[3]{\frac{\sum(n_i \times D_i^3)}{n_i}}$, the polydispersity index $PDI(TEM) = D_w/D_n$ were calculated [30].

Size exclusion chromatography (SEC). The polymer molecular weight and its dispersity were measured by SEC (Agilent 1260 Infinity) using tetrahydrofuran as eluent. The system was packed with a set of analytical and guard columns (Polymer Laboratories ResiPore, nominal particle size: 3 μm ; porosity, two columns (300 \times 7.5 mm) and one guard column (50 \times 7.5 mm)). The solvent flow rate was set to 1 mL/min, thermally controlled at 35°C. The system was then calibrated with universal calibration standard (EasiVial polystyrene standards, Agilent) using multi-detectors (refractive index, viscosity and ultra-violet detectors). Agilent GPC/SEC software was used to obtain the molecular weight data.

Results and discussion

1. Influence of monomer water solubility on particle size

N_p being determined from particle size measurements, our first approach has been to assess the change of particle size as a function of the water solubility of thiol and ene monomers. A series of experiments was thus carried out by polymerizing in emulsion diallyl phthalate (**DAP**) with six different dithiols whose water solubility (s) follows the order:

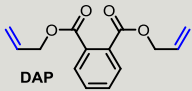
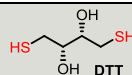
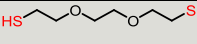
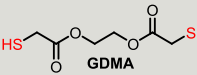
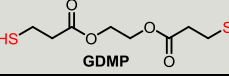
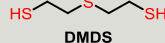
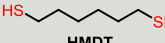
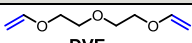
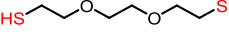
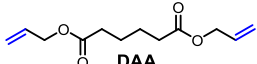
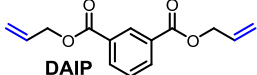
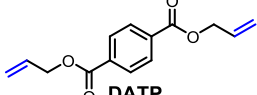
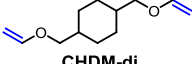
DL-dithiothreitol (**DTT**) > 2,2-(ethylenedioxy)diethanedithiol (**EDDT**) > ethylene glycol bismercaptoacetate (**GDMA**) > ethylene glycol bis(3-mercaptopropionate) (**GDMP**) > 2,2'-thioldiethanethiol (**DMDS**) > 1,6-hexanedithiol (**HMDT**).

In a second series, the dithiol **EDDT** was fixed and polymerized with six different dienes of water solubility decreasing in the order:

di(ethylene glycol) divinyl ether (**DVE**) > diallyl adipate (**DAA**) > diallyl phthalate (**DAP**) > diallyl isophthalate (**DAIP**) > diallyl terephthalate (**DATP**) > 1,4-bis[(vinyl)oxy]methyl]cyclohexane (**CHDM**).

In all runs, the SDS concentration was kept constant at 13.2 mM (above CMC). The thiol-ene emulsions were irradiated for 20 min ($\lambda = 385$ nm) in the presence of a water soluble radical photoinitiator ([TPO-Li] = 7.5 mM). At the end of each reaction, conversion in ene functional group (NMR data), molecular weight (SEC data), and particle size (z-average diameter D_z (DLS), DLS data) were determined. The chemical structures of the monomers, their water solubility and the polymer characteristics were gathered in **Table 1**. The water-solubility values were obtained from various sources (see **Table S1** of SI for details), and are based solely on the pure monomer in water. Cross-coupling effects between the solubilities of thiol and ene compounds are thus neglected.

Table 1. Influence of monomer water solubility on particle size during dithiol-diene step polymerization in emulsion. [SDS] = 13.2 mM, [TPO-Li] = 7.5 mM, [monomers] = 10 wt%, irradiation time = 20 min, $\lambda_{\max} = 385$ nm, irradiance = 3.7 mW cm⁻². Conversions in all cases are > 95%.

Diene	S_{diene}^a mM	Dithiol	S_{dithiol}^a mM	\overline{M}_n^b kg mol ⁻¹	D^b	$D_z(\text{DLS})^c$ nm
 DAP	0.46 ± 0.27	 DTT	5.1 × 10 ³	5.5	2.6	187 ± 7
		 EDDT	72 ± 10	13.5	2.8	98 ± 3
		 GDMA	67 ± 28	6.7	2.3	69 ± 3
		 GDMP	15.0 ± 0.8	4.5	2.0	118 ± 4
		 DMDS	4.0 ± 0.1	9.3	2.4	77 ± 2
		 HMDT	1.4 ± 0.4	7.6	2.9	53 ± 2
 DVE	86.6 ± 0.6	 EDDT	72 ± 10	9.1	1.8	185 ± 5
 DAA	5.1			5.4	2.1	111 ± 1
 DAIP	0.2			10.9	4.0	103 ± 4
 DATP	0.17			10.4	2.3	67 ± 4
 CHDM-di	0.13			6.2	1.9	64 ± 1

^a Water solubility data were obtained from different sources (see **Table S1** in SI). ^b \overline{M}_n and D were determined by SEC in THF. ^c z-average diameter D_z (DLS) was determined by DLS.

The number-average molecular weight \overline{M}_n of the latexes ranges from 4.5 to 13.5 kg mol⁻¹, while the molecular weight dispersity D spans from 2 to 4. All the polymers have thus a sufficiently high molecular weight showing the viability of the process. The reasons for the variability in molecular weight are related to slight

differences of monomer conversion (in the range 95–100 %) and the difficulty to obtain an accurate stoichiometric amount of functional groups. Our primary point of interest remains the evolution of particle size. As can be seen in **Table 1**, it should be pointed out the greater tendency to form smaller particles when decreasing the water solubility of the thiol or the ene monomer. For example, for the first series of **DAP**-dithiol emulsions, $D_z(DLS)$ decreases from 187 nm with completely water soluble dithiol **DTT** to less than 100 nm for dithiols with very limited water solubility including **DMDS** ($s = 4.0$ mM) and **HMDT** ($s = 1.4$ mM). Although there is an exception to this generalization (case of **DAP-GDMP**), this overall behavior also applies to the second series of latexes involving **EDDT** with various dienes. Depending on the polarity (water solubility) of the monomer used, the concentration of surfactant adsorbed at the water/particle changes, and generally tends to decrease with a greater hydrophilicity of the monomers [2, 17]. The lower surfactant equilibrium concentration at the surface of more polar particles causes a poorer surface coverage, making particles more susceptible to coalescence to form larger particles. The driving force for coagulation of instable smaller-sized particles into stable larger (mature) particles is the increase of the total polymer particle surface. The greater tendency for the occurrence of a *coagulative nucleation* mechanism with more water soluble monomers agrees with the behavior described in chain radical polymerization [14].

2. Dependence of N_p on surfactant concentration

2.1 Accurate particle size and N_p measurements

A step forward to study particle nucleation is to investigate N_p as a function of [S]. N_p being dependent on the 3-power of the particle diameter, the access to accurate particle size data is an important condition to obtain reliable N_p values. Because a typical N_p vs [S] plot requires a minimum of 15-20 points, we have found more practical to use DLS as mainstream technique to determine particle size for particle number calculation. To assess the reliability and accuracy of DLS data, these latter were compared to size data given by cryo-TEM. Though cryo-TEM requires more complex specimen preparation, it is the only technique able to image nanoparticles in their native form and provides reliable particle size. For sake of clarity, we have limited our comparison to three latexes prepared by polymerizing **DAP** with three dithiols of different water solubility: **EDDT** (high s), **DMDS** (medium s), **HMDT** (low s). In all formulations, the same concentration of SDS (20 mM) was used. **Table 2** shows for DLS and cryo-TEM the number-average diameter D_n (primary parameter provided by cryo-TEM), weight-average diameter D_w , z-average diameter D_z (primary parameter provided by DLS), volume-average diameter D_v , the polydispersity index PDI . The relationships to obtain the different average diameters are given in the experimental section. There is a reasonable accord between DLS and cryo-TEM average diameters. Only the **DAP-HMDT** latex shows a significant difference between $D_z(TEM) = 26$ nm and $D_z(DLS) = 38$ nm. It is common to obtain larger $D_z(DLS)$ values than $D_z(TEM)$ values [30]. The significant deviation found in **DAP-HMDT** is explained by the increased polydispersity index of DLS results compared to the other samples. The result from a DLS experiment ($D_z(DLS)$) is primarily an intensity distribution that is thus more weighted by the larger particles due to their higher scattering coefficients. A broader size distribution means a strong dependence of the detector-response with respect to the large

particles, resulting in larger $D_z(DLS)$ values. Therefore, it is likely that cryo-TEM provides a better overview of particle dispersity. In this respect, **Figure 2** shows for each **DAP** based latex a cryo-TEM image and the corresponding size distribution. **DAP-EDDT** latex has a significantly broader particle size distribution ($PDI(cryo - TEM) = 1.36$) compared to **DAP-DMDS** and **DAP-HMDT** systems ($PDI(cryo - TEM) \sim 1.27$). This results supports a more extensive coagulative nucleation mechanism when the polymerization involves a water soluble monomer (**EDDT**).

Table 2. Particle average diameters for set of three **DAP**-based latexes prepared at [SDS]= 20 mM.

	$D_n(DLS)$ nm	$D_v(DLS)$ nm	$D_w(DLS)$ nm	$D_z(DLS)$ nm	$PDI(DLS)$	$D_n(cryo-TEM)$ nm	$D_v(cryo-TEM)$ nm	$D_w(cryo-TEM)$ nm	$D_z(cryo-TEM)$ nm	$PDI(cryo-TEM)$
DAP-EDDT	59 ± 5	68 ± 5	92 ± 1	99 ± 1	1.55 ± 0.13	61 ± 1	69	83	96	1.36
DAP-DMDS	35 ± 2	39 ± 2	49 ± 1	57 ± 1	1.67 ± 0.08	37 ± 1	40	47	56	1.27
DAP-HMDT	17 ± 1	21 ± 1	31 ± 1	38 ± 1	1.82 ± 0.07	18 ± 1	20	23	26	1.28

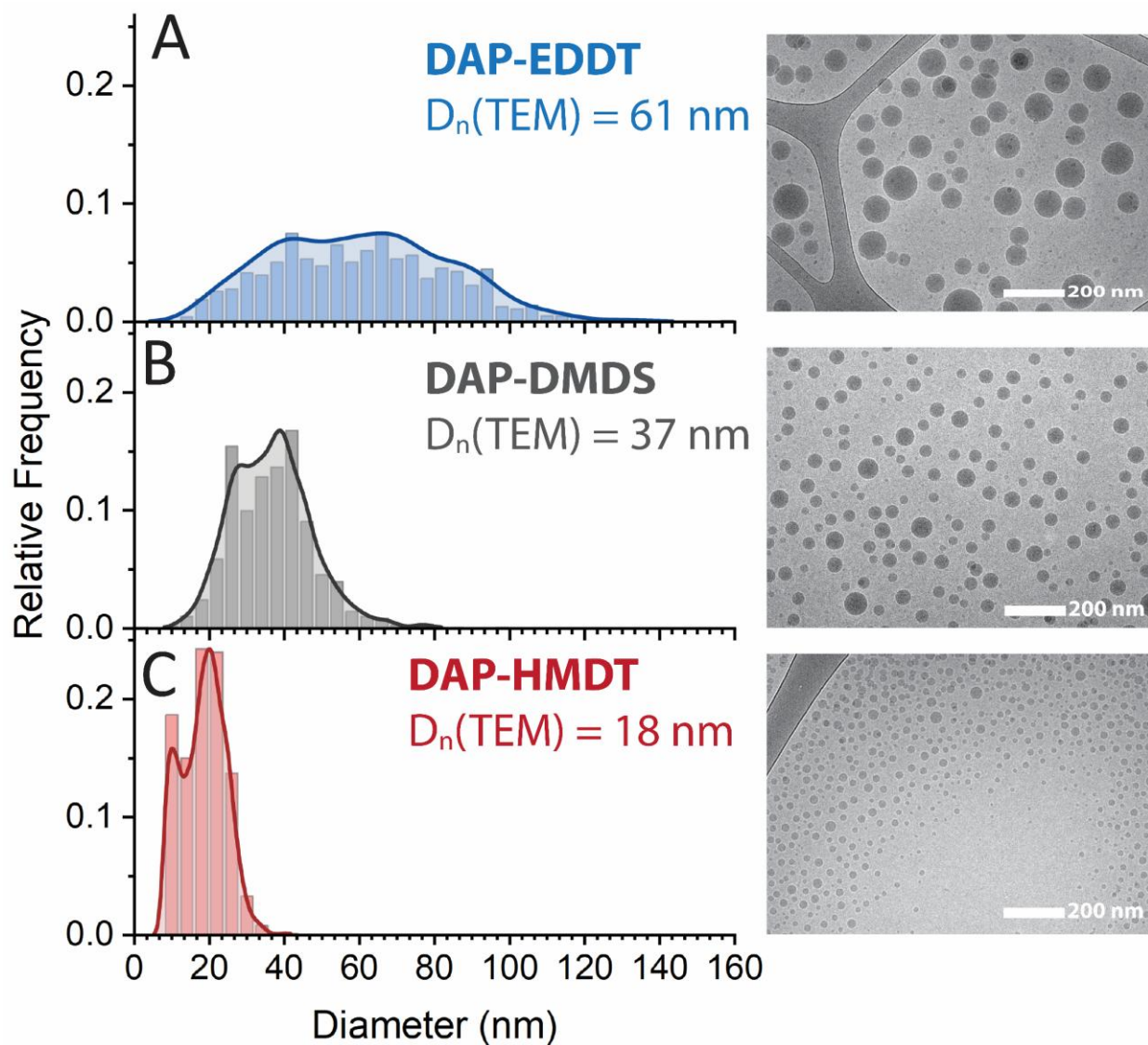


Figure 2. Cryo-TEM image and corresponding particle size distributions of three latexes prepared at $[\text{SDS}] = 20 \text{ mM}$ by emulsion thiol-ene polymerization. Data were fitted with kernel density estimation functions. In all cases the bin size is 4 nm, and Scott's rule was used to determine the bandwidth. Histograms are based on analysis of 1089 particles (A: **DAP-EDDT**), 1192 particles (B: **DAP-DMDS**) and 2845 particles (C: **DAP-HMDT**).

2.2 N_p vs $[\text{S}]$ plot

Having proved the reliability of the size data obtained by DLS, N_p was calculated from $D_p(\text{DLS})$ values for latexes produced over a range of SDS concentrations spanning from 0.1 mM to 200 mM. As shown in **Figure 3**, three separate sets of experiments were conducted using a given ene (**DAP**, **DVE** or **CHDM**) and the same three dithiols used previously: **EDDT** (high s), **DMDS** (medium s), **HMDT** (low s). The advantages of using these three diene is to investigate also the effect of ene water solubility which follows the decreasing order: $s(\text{DVE}) < s(\text{DAP}) < s(\text{CHDM})$.

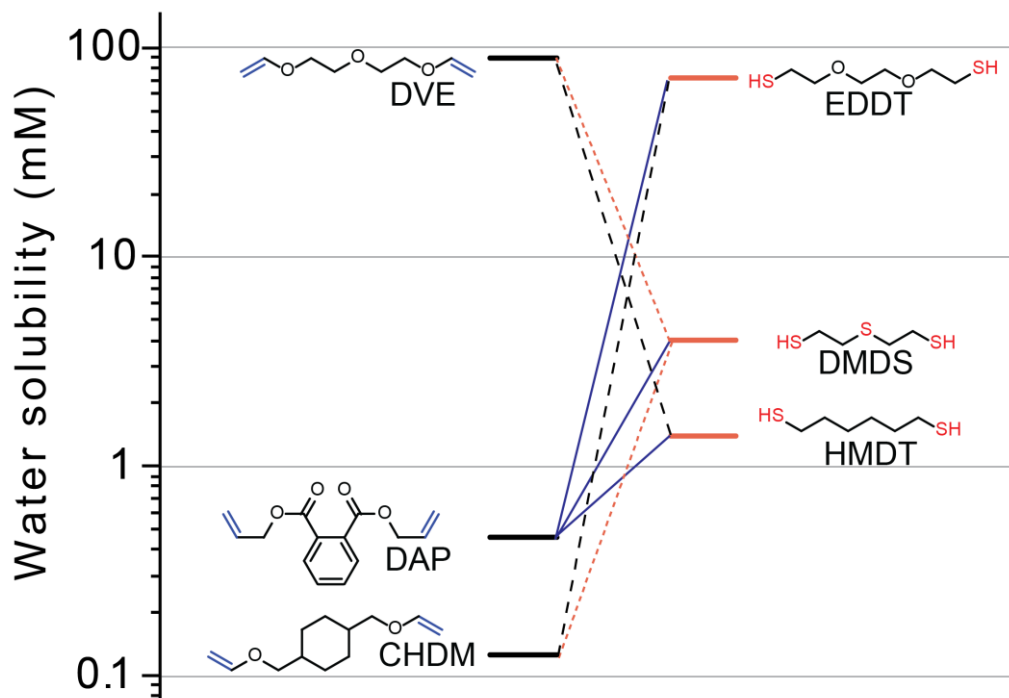


Figure 3. Water solubility of various diene and dithiol monomers used in thiol-ene emulsion step polymerizations.

a. Case of DAP-dithiol

Figure 4 is a plot of N_p as a function of [SDS] in logarithmic scale for the three latexes **DAP-EDDT**, **DAP-DMDS** and **DAP-HMDT**. Regardless of the thiol used, it is clear that the plot $N_p \propto [\text{SDS}]^x$ cannot be fitted by a single exponent of x . The typical sigmoidal shape observed in conventional radical chain polymerizations is found, where four regimes depending on the surfactant concentration can be distinguished, each characterized by a different x value.

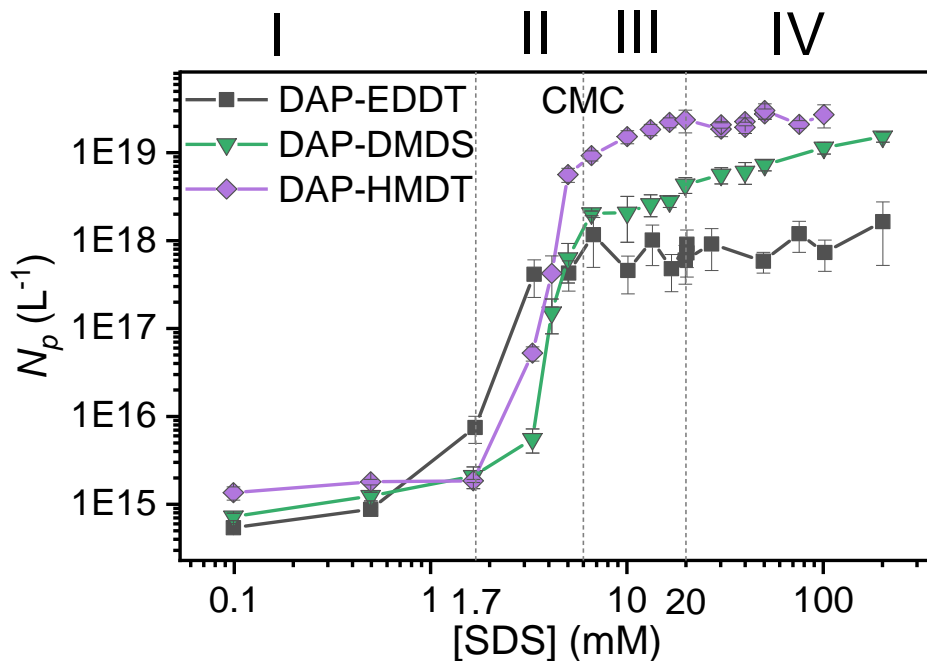


Figure 4. Particle number as a function of [SDS] for **DAP**-dithiol emulsion polymerization using a logarithmic scale on the x -axis and the y -axis.

Obviously, for $0.1 \text{ mM} < [\text{SDS}] < 2 \text{ mM}$ (**region I**), the surfactant has negligible effect on N_p ($x = 0$) and homogeneous nucleation is the only active mechanism. There is a sudden change in N_p when [SDS] is near the CMC, which is particularly evident for monomers with intermediate and low water solubility such as **DMDS** and **HMDT**. The spike in N occurs at [SDS] of about 3 to 6 mM (**region II**). This agrees with the CMC value of SDS reported in literature which varies in a wide range from 1.7 to 9 mM. In this study, we chose a CMC of SDS at 6 mM in agreement with the value reported by Sütterlin [18, 20, 31]. In addition, this second region is also marked by a change of the latex optical properties, from turbid to translucent (**Figure 5**). The lower the water solubility of the thiol monomer (the hydrophilicity of the polymer), the steeper the increase in particle number near the CMC. Such steep rise in N_p might be accounted for the occurrence of a second mode of particle formation by micellar nucleation.



Figure 5. Photos of a **DAP-HMDT** latex prepared with increasing SDS concentrations, from left to right the concentration of SDS was increased in the range of 0.1-200 mM.

At $\text{CMC} < [\text{SDS}] < 3\text{-}4 \text{ CMC}$ (6-20 mM) (**region III**), the three systems show different behaviors. With **DAP-EDDT** system, N_p is relatively independent of $[\text{SDS}]$ ($x = 0.17 \pm 0.09$) as reported previously [26]. In contrast, the **DAP-DMDS** and **DAP-HMDT** systems exhibit a steady increase of N_p vs $[\text{SDS}]$, with $x = 0.65 \pm 0.04$ and 0.77 ± 0.08 , respectively. Note that a power law fitting is the only appropriate model to fit the experimental data in this region (The fitting methods are detailed in **Fig. S3** of SI). Clearly, the exponent x tends to decrease with increasing thiol water solubility. This reflects a growing agglomeration tendency due to a reduced effectiveness of adsorption on particle surface. As explained previously, the surface concentration of surfactant molecule (Γ , in mol/cm^2) is likely to be smaller on a more hydrophilic polymer particle surface which disfavors the packing of surfactant necessary to obtain minimum particle size. One can draw a parallel with an emulsion chain polymerization for which a similar tendency has been reported [18, 31, 32]. For SDS larger than 20 mM, the general behavior of **DAP-DMDS** and **DAP-EDDT systems** remain similar over a broad range of concentrations, leading to a similar exponent x value. By contrast, x decreases significantly in the case of **DAP-HMDT** ($x = 0.13 \pm 0.10$) at larger surfactant concentration, forcing us to create a **region IV** ($[\text{SDS}] > 20 \text{ mM}$). Above CMC, it is therefore not possible to find a single and general fitting of $N_p = f([\text{SDS}])$. Therefore, in the rest of the study, we have focused on region III ($\text{CMC} < [\text{SDS}] < 3\text{-}4 \text{ CMC}$) to study more comprehensively the effect of monomer solubility on the exponent x value. Though limited in terms of surfactant concentration (6-20 mM), this range is the most widely used in emulsion polymerization and a minimum of five points were used for curve fitting.

b. Cases of CHDM-dithiol and DVE-dithiol

We have investigated the dependence of N_p as a function of $[\text{SDS}]$ in region III only for latexes prepared with two other dienes: **CHDM** (less water soluble than **DAP**) and **DVE** (more water soluble than **DAP**) (Figure 3). In each case, the diene was polymerized with the same three thiols (**EDDT**, **DMDS** and **HMDT**). The $N_p \propto [\text{SDS}]^x$ plots shown in **Figure 6** all exhibit a sigmoidal shape. We have focused our attention on the **region III** ($20 \text{ mM} > [\text{SDS}] > 6 \text{ mM}$). Interestingly, x remains at a high level for the three latexes prepared with **CHDM** whatever the thiol used: $x = 0.75 \pm 0.04$ (**EDDT**), $x = 1.05 \pm 0.14$ (**DMDS**) and $x = 0.96 \pm 0.12$ (**HMDT**). It is apparent that even with **EDDT** the most water soluble thiol, step polymerization with highly water-insoluble **CHDM** drives a sufficiently low polar particle surface to allow the surfactant adsorption, resulting in a high value of x , and consequently a progressive increase of N_p when more surfactant is present. Conversely, when choosing the more water soluble **DVE**, there is no clear dependence of N_p on $[\text{SDS}]$ at above CMC for thiols **EDDT** ($x < 0$) and **DMDS** ($x = 0.21 \pm 0.12$). The reduced adsorption efficiency of SDS on the more polar surface results in a higher agglomeration tendency, and the incapacity for more surfactant molecules to adsorb onto particle surface to further reduce particle size. Only the copolymerization of **DVE** with the most water-insoluble **HMDT** enables to rise the adsorption effectiveness, resulting in a x value of 0.66 ± 0.12 .

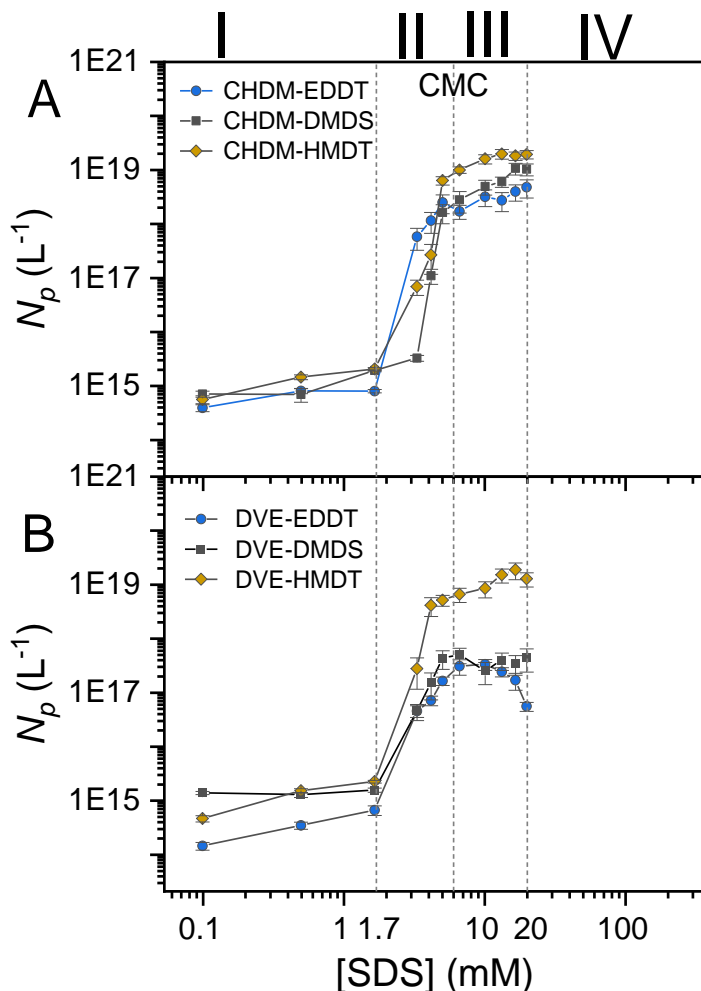
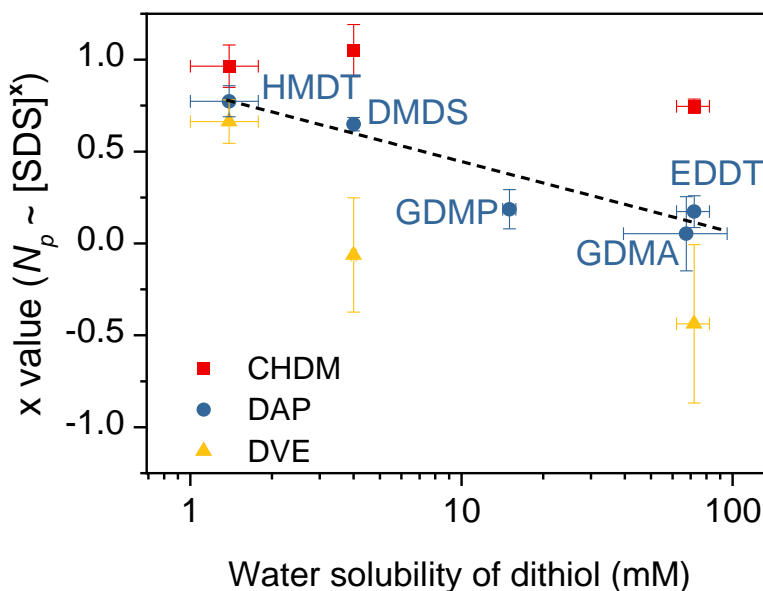


Figure 6. Particle number as a function of [SDS] for latexes prepared by emulsion polymerization of **CHDM** (A) and **DVE** (B) with three different dithiols: **EDDT**, **DMDS** and **HMDT** using a logarithmic scale on the x-axis and the y-axis.

2.3 Effect of monomer solubility on the dependence of N_p on [S] above CMC (region III)

We finally tried to correlate the values of the exponent x above CMC (in region III) with the monomer water solubility. For this purpose, **Figure 7** shows on a single graph the values of x obtained with latexes prepared with a broad range of thiol and ene monomers. The data were obtained by polymerizing the three dienes **CHDM** (low s), **DAP** (medium s) and **DVE** (high s) with a range of dithiols of decreasing water solubility: **EDDT** > **GDMA** > **GDMP** > **DMDS** > **HMDT**. The case of **DAP** presenting a medium polarity is interesting since there is a general trend showing a gradual decrease of x from 0.77 ± 0.08 to 0 when increasing thiol polarity. In addition, the combination of two highly water-insoluble co-monomers (*e.g.* **CHDM-HMDT**) drives a high value of $x = 0.96 \pm 0.12$, whereas the polymerization of two water soluble monomers (*e.g.* **DVE-EDDT**) gives a value close to zero or even negative. However, the interplay between monomer solubility and x in a thiol-ene emulsion polymerization is more complex when the two co-monomers have opposite water solubility. This result is consistent with the fact that

the copolymer chains contain as structural repeating unit the addition reaction of dithiol with diene, so both comonomers can affect to a certain extent the polarity of the polymer, resulting in different surfactant adsorption and particle size. Importantly, when the monomer mixture contains at least a highly water-insoluble component, whether thiol or ene (e.g. **CHDM** or **HMDT**), it is experimentally found that a relatively high x value can be achieved even in the presence of a highly water soluble counter-part, such as **DVE** ene or **EDDT** thiol. Thus, one can find $x = 0.75$



± 0.04 with the couple **CHDM-EDDT** or $x = 0.66 \pm 0.12$ with **DVE-HMDT**.

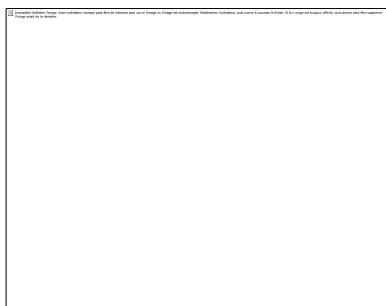
Figure 7. Dependence of exponents x of ($N_p \propto [\text{SDS}]^x$) in the region III ($[\text{SDS}] > \text{CMC}$) depending on the water solubility of the dithiol and diene monomer.

Conclusion

To gain a better understanding of particle formation in an emulsion step polymerization, the effect of monomer polarity on the final particle size was studied during the photopolymerization of an emulsion based on dithiol and diene monomers. Above the CMC, particle size decreased with the water insolubility of the monomers due to the better surface coverage of surfactant on less polar surface. The dependence of N_p on $[\text{S}]$ was calculated based on dynamic light scattering data (using volume-average diameters). The evolution of N_p was plotted against $[\text{SDS}]$ for different thiol-ene couples. Regardless of the monomer water solubility, the plot $\log N_p$ vs $\log [\text{S}]$ had a sigmoidal shape indicative of three regions following distinct $N_p \propto [\text{SDS}]^x$ relationships. At low surfactant concentration (below CMC), N_p hardly changed and x approached zero. In the vicinity of the CMC, a large change in N_p was observed. In the range $\text{CMC} < [\text{S}] < 3\text{-}4 \times \text{CMC}$, high values of x ($0.6 - 1$) were found provided that at least one of the two co-monomers was water-insoluble. Systematically, the association of two water-insoluble co-

monomers resulted in high x values, while two water soluble co-monomers led to values close to zero. This overall behavior bears a strong resemblance with that reported in a conventional emulsion chain polymerization where the exponent x above the CMC is known to decrease with increasing the monomer polarity. This study provides both a practical approach to control particle size in emulsion step polymerization and shows that fundamental mechanism underlying particle formation mechanism does not change significantly when changing the polymerization mechanism.

Graphical abstract



Acknowledgements

This project has received funding from the European Union’s Horizon 2020 research and innovation programme under the Marie Skłodowska-Curie grant agreement n° 765341 (project photo-emulsion, MSCA-ITN-2017).

Conflict of Interest

The authors declare no conflicts of interest

Abbreviations and Symbols

Abbreviations and symbols	Definition	Classification
N_p	Number of particle per unit volume (L^{-1})	
[S]	Surfactant concentration ($mol L^{-1}$)	
[I]	Initiator concentration ($mol L^{-1}$)	
CMC	Critical Micelle Concentration	
SEC	Size exclusion chromatography	
D_z	z-average diameter	
D_w	Weight-average diameter	Particle characterization terms
D_v	Volume-average diameter	

D_n	Number-average diameter	
DLS	Dynamic light scattering	
cryo-TEM	Cryogenic transmission electron microscopy	
S_{diene}	Water-solubility of diene	
$S_{dithiol}$	Water-solubility of dithiol	
DAP	Diallyl phthalate	
DATP	Diallyl terephthalate	
DAIP	Diallyl isophthalate	Diene
DAA	Diallyl adipate	
DVE	Di(ethylene glycol) divinyl ether	
CHDM	1,4-Bis[(vinyl)oxy)methyl]cyclohexane	
EDDT	2,2-(Ethylenedioxy)diethanedithiol	
DTT	DL-dithiothreitol	
GDMA	Ethylene glycol bis(mercaptoacetate)	
GDMP	Ethylene glycol bis(3-mercaptopropionate)	Dithiol
DMDS	2,2'-Thioldiethanethiol	
HMDT	1,6-Hexanedithiol	
DBHQ	2,5-Di-tert-butylhydroquinone	Radical inhibitor
SDS	Sodium dodecyl sulfate	Surfactant
TPO-Li	Lithium phenyl(2,4,6-trimethylbenzoyl)phosphinate	Water-soluble photoinitiator

References

- [1] Tauer K, Kühn I (1997) in Asua JM (ed) *Polymeric Dispersions: Principles and Applications* Springer Netherlands, Dordrecht, pp 49-65
- [2] Fitch RM (1980) *Polymer Colloids II*. Springer Science & Business Media, New York
- [3] Sood A (2008) Modeling of the particle size distribution in emulsion polymerization. *J Appl Polym Sci.* 109: 1403-1419. <https://doi.org/10.1002/app.28083>
- [4] Lovell PA, Schork FJ (2020) Fundamentals of Emulsion Polymerization. *Biomacromolecules.* 21: 4396-4441. <https://doi.org/10.1021/acs.biomac.0c00769>
- [5] Fitch RM, Tsai CH (1971) in Fitch RM (ed) *Polymer Colloids* Springer US, Chicago, Illinois
- [6] Hansen FK, Ugelstad J (1978) Particle nucleation in emulsion polymerization. I. A theory for homogeneous nucleation. *J Polym Sci, Polym Chem Ed.* 16: 1953-1979. <https://doi.org/10.1002/pol.1978.170160814>
- [7] Dunn AS (1989) Latex particle nucleation in emulsion polymerization. *Eur Polym J.* 25: 691-694. [https://doi.org/10.1016/0014-3057\(89\)90030-x](https://doi.org/10.1016/0014-3057(89)90030-x)
- [8] Morrison BR, Maxwell IA, Gilbert RG, Napper DH (1992) *Polymer Latexes*, pp 28-44
- [9] Chern CS, Liou YC, Chen TJ (1998) Particle nucleation loci in styrene miniemulsion polymerization using alkyl methacrylates as the reactive cosurfactant. *Macromol Chem Phys.* 199: 1315-1322. [https://doi.org/10.1002/\(sici\)1521-3935\(19980701\)199:7<1315::aid-macp1315>3.0.co;2-9](https://doi.org/10.1002/(sici)1521-3935(19980701)199:7<1315::aid-macp1315>3.0.co;2-9)
- [10] Nazaran P, Tauer K (2007) Nucleation in Emulsion Polymerization: Another Step towards Non-Micellar Nucleation Theory. *Macromol Symp.* 259: 264-273. <https://doi.org/10.1002/masy.200751331>

- [11] Tauer K, Hernández HF, Kozempel S, Lazareva O, Nazaran P (2007) Adaption of the Mechanism of Emulsion Polymerization to New Experimental Results. *Macromol Symp.* 259: 253-263. <https://doi.org/10.1002/masy.200751330>
- [12] Tauer K, Hernandez H, Kozempel S, Lazareva O, Nazaran P (2008) Towards a consistent mechanism of emulsion polymerization-new experimental details. *Colloid Poly Sci.* 286: 499-515. <https://doi.org/10.1007/s00396-007-1797-3>
- [13] Tauer K, Nazaran P (2010) Mechanism and Modeling of Emulsion Polymerization: New Ideas and Concepts - 1. Particle Nucleation. *Macromol Symp.* 288: 1-8. <https://doi.org/10.1002/masy.201050201>
- [14] Dobrowolska ME, van Esch JH, Koper GJ (2013) Direct visualization of "coagulative nucleation" in surfactant-free emulsion polymerization. *Langmuir.* 29: 11724-11729. <https://doi.org/10.1021/la4027927>
- [15] Smith WV, Ewart RH (1948) Kinetics of Emulsion Polymerization. *J Chem Phys.* 16: 592-599. <https://doi.org/10.1063/1.1746951>
- [16] Fitch RM (1973) The homogeneous nucleation of polymer colloids. *Br Polym J.* 5: 467-483. <https://doi.org/10.1002/pi.4980050606>
- [17] Gardon JL (1968) Emulsion polymerization. II. Review of experimental data in the context of the revised Smith-Ewart theory. *J Polym Sci, Part A-1: Polym Chem.* 6: 643-664. <https://doi.org/10.1002/pol.1968.150060319>
- [18] Sütterlin N (1980) *Polymer Colloids II* Springer, New York, pp 583-597
- [19] Daniels ES, Sudol ED, El-Aasser MS (1992) in Comstock MJ (ed) *ACS Symposium* Washington, DC (United States); American Chemical Society, Washington, DC
- [20] Krishnan S, Klein A, El-Aasser MS, Sudol ED (2003) Effect of Surfactant Concentration on Particle Nucleation in Emulsion Polymerization of n-Butyl Methacrylate. *Macromolecules.* 36: 3152-3159. <https://doi.org/10.1021/ma021120p>
- [21] Czajka A, Armes SP (2021) Time-Resolved Small-Angle X-ray Scattering Studies during Aqueous Emulsion Polymerization. *J Am Chem Soc.* 143: 1474-1484. <https://doi.org/10.1021/jacs.0c11183>
- [22] Subervie D, Le Quémener F, Canterel R, et al. (2021) Visible-Light Emulsion Photopolymerization of Acrylates and Methacrylates: Mechanistic Insights and Introduction of a Simplified Sulfur-Based Photoinitiating System. *Macromolecules.* <https://doi.org/10.1021/acs.macromol.0c01692>
- [23] Galanopoulo P, Gil N, Gignes D, et al. (2022) One-Step Synthesis of Degradable Vinilic Polymer-Based Latexes via Aqueous Radical Emulsion Polymerization. *Angew Chem Int Ed Engl.* <https://doi.org/10.1002/anie.202117498>
- [24] Jönsson JB, Müllner M, Piculell L, Karlsson OJ (2013) Emulsion Condensation Polymerization in Dispersed Aqueous Media. Interfacial Reactions and Nanoparticle Formation. *Macromolecules.* 46: 9104-9113. <https://doi.org/10.1021/ma401799g>
- [25] Durham OZ, Chapman DV, Krishnan S, Shipp DA (2017) Radical Mediated Thiol-Ene Emulsion Polymerizations. *Macromolecules.* 50: 775-783. <https://doi.org/10.1021/acs.macromol.6b02228>
- [26] Le CMQ, Schmutz M, Chemtob A (2020) Ab Initio Batch Emulsion Thiol-Ene Photopolymerization. *Macromolecules.* 53: 2369-2379. <https://doi.org/10.1021/acs.macromol.0c00265>
- [27] Durham OZ, Shipp DA (2020) Polymer Colloids from Step-Growth Thiol-X Polymerizations. *Polymer Reviews.* 61: 54-79. <https://doi.org/10.1080/15583724.2020.1743307>
- [28] Rocha- Botello G, Olvera- Guillen R, Herrera- Ordonez J, Cruz- Soto M, Victoria- Valenzuela D (2019) Unexpected Secondary Nucleation in Poly(Vinyl acetate) Nanoparticle Synthesis by Ab Initio Batch Emulsion Polymerization Using Poly(Vinyl alcohol) as Surfactant. *Macromol React Eng.* 13. <https://doi.org/10.1002/mren.201900024>
- [29] Jansen TGT, Meuldijk J, Lovell PA, van Herk AM (2015) On the Reaction Characteristics of Miniemulsion Polymerization with Aqueous Phase Initiation - Experiments and Modeling. *Macromol React Eng.* 9: 19-31. <https://doi.org/10.1002/mren.201400025>

- [30] Durrieu V, Putaux J-L, Passas R, Gandini A (2004) Cryo-TEM and Image Analysis of Polymer Nanoparticle Dispersions. *Cryoelectron Microscopy*. 18: 19-21. Doi:<https://hal.archives-ouvertes.fr/hal-02109636>
- [31] Sütterlin N, Kurth H-J, Markert G (1976) Ein Beitrag zur Teilchenbildung bei der Emulsionspolymerisation von Acrylsäure- und Methacrylsäureestern. *Makromol Chem*. 177: 1549-1565. <https://doi.org/10.1002/macp.1976.021770523>
- [32] Van Der Hoff BME (1962) in Platzner NAJ (ed) *Polymerization and Polycondensation Processes*, 34 edn. American Chemical Society, Washington, D.C., pp 6-31